THE JOURNAL OF PHYSICAL CHEMISTRY B
A JOURNAL OF THE AMERICAN CHEMICAL SOCIETY

pubs.acs.org/JPCB

Article

Dynamics of Deep Eutectic Mixtures of Tetraethylammonium Halides/Ethylene Glycol Investigated with Ultrafast Infrared Spectroscopy

Published as part of The Journal of Physical Chemistry B special issue "Mark A. Johnson Festschrift".

Junkun Pan,[‖] Kimberly A. Carter-Fenk,[‖] Samantha T. Hung, Nhu Dao, Jordyn N. S. Smith, and Michael D. Fayer*

Cite This: https://doi.org/10.1021/acs.jpcb.4c08739

Read Online

ACCESS | Metrics & More | Article Recommendations

ABSTRACT: Health and environmental risks posed by volatile organic solvents create an incentive to develop safer, less volatile solvents with the appropriate functionality. Deep eutectic solvents and other low-volatility organic mixtures offer a highly tunable alternative through a mixture composition selection. However, a significant gap exists in understanding the relationship between molecular-level properties and the resulting solvation and transport properties. Using ultrafast infrared (IR) polarization-selective pump−probe (lifetimes and orientational relaxation) spectroscopy, we investigated the dynamics of 1:3 molar mixtures of tetraethylammonium bromide (TEABr) and chloride (TEACl) with ethylene glycol (EG) and of pure EG using the anionic vibrational probe, the CN stretch of $SeCN^-$. The very high salt concentrations are in many respects analogous to water-in-salt solutions, e.g., LiBr and LiCl. These ion/water mixtures can have extremely high ratios of ions to solvating neutral molecules, similar to the 1:3TEABr and 1:3TEACl mixtures studied here. In 1:3TEABr/EG and 1:3TEACl/EG solutions, there are far too few EGs to solvate the ions. Therefore, like water-in-salt, 1:3TEABr/EG and 1:3TEACl/EG solutions will have solvent-separated ion pairs, contact ion pairs, and large ion/EG clusters, forming extended ion/solvent networks. The orientational dynamics experiments on 1:3TEABr/EG and 1:3TEACl/EG show striking similarities to experiments from the literature on 1:4 LiBr and LiCl aqueous solutions, even though the cations and solvents in the deep eutectic mixtures are vastly different.

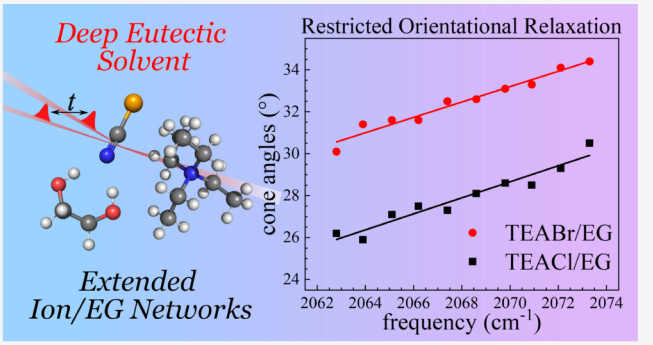

1. INTRODUCTION

Volatile organic solvents are ubiquitous in industrial processes and chemical laboratories. Increasing attention is being placed on identifying suitable nonvolatile and low-volatility solvents to reduce air pollution and deleterious health effects associated with the evaporation of volatile organic compounds.[1−4] Replacing conventional solvents with less volatile alternatives with comparable solvation properties has been challenging, and only a limited number of molecular liquids meet the demands of both performance and sustainability.[5]

Solvents comprised of molecular mixtures can provide added flexibility in tuning desirable physicochemical and solvation properties for improved safety, sustainability, reaction, and catalysis optimization.[6,7] Predicting and modeling physicochemical properties of liquid mixtures from first principles is a formidable task,[8] and experimentally determining the nature of molecular-level structures, dynamics, and intermolecular interactions that give rise to macroscopic liquid properties is challenging.[9,10] Consequently, most solvent mixtures have been developed through trial and error. Characterization of intermolecular interactions and solute dynamics in low-volatility organic liquid mixtures is needed to increase the efficacy of solvent development through an improved understanding of the microscopic structural dynamics driving thermodynamic and transport properties.

A growing body of scientific literature has investigated intermolecular interactions and solvation in low-volatility mixtures through time-resolved spectroscopies and computational studies.[9] Many studies have focused on deep eutectic

Received: December 27, 2024
Revised: February 15, 2025
Accepted: February 21, 2025

solvents (DESs), a novel class of liquids prepared by mixing at least two constituents: a hydrogen bond acceptor (HBA), often comprising a quaternary ammonium salt or a metal chloride hydrate, and a hydrogen bond donor (HBD), typically an organic molecular component. The mixtures are characterized by an anomalously low eutectic point compared to the ideal mixture's predicted eutectic point.[9,11] While DESs share many physicochemical properties with ionic liquids, such as a wide liquid range, low volatility, low vapor pressure, high thermal stability, and tunable polarity, the individual constituents in DESs are not always ionic.[9,11,12]

The mixture composition and molecular properties of the HBDs and HBAs provide a convenient handle for tuning the DES properties. Spittle et al. recently demonstrated faster solvation dynamics and increased direct-current ionic conductivity within the eutectic composition range of choline chloride and ethylene glycol mixtures, highlighting the influence of mixture composition and dynamics on the transport properties of the macroscopic liquids.[13] Other studies of DES have investigated how HBD structure and functional groups impact intermolecular interactions, dynamics, and viscosity.[14−22] For example, Chowdhury et al. observed that hydrogen bond (H-bond) dynamics correlate with bulk liquid viscosity for mixtures of ethylene glycol, glycolic acid, and malonic acid with choline chloride, and the presence of spatially heterogeneous nanodomains throughout the liquid mixture exhibits variations in the contributions of H-bond dynamics to the overall bulk liquid viscosity.[18] Less focus has been placed on HBAs, specifically, the anions that act as HBAs in some DESs, despite their importance in the resulting structural and H-bonding in DESs.[23−25] H-bond accepting anions are particularly important in applications such as processing natural polymers like cellulose, lignocellulose, and chitin.[26−29] Therefore, understanding how HBA anions affect intermolecular interactions and dynamics within liquid mixtures is useful.

Ethylene glycol-based eutectic mixtures have garnered significant interest due to their relatively low viscosities and improved transport properties relative to other DESs.[30] Ethaline, a mixture of ethylene glycol and choline chloride, has attracted the most attention. However, recent work has shown that ethaline only exhibits an ideal thermodynamic melting point depression, not an anomalously low eutectic point that defines a DES.[31] Ethylene glycol and quaternary ammonium mixtures are useful and well-characterized model compounds to analyze how hydrogen bond donor and acceptor structures and compositions impact solvent intermolecular interactions and dynamics. Desirable properties associated with DESs are not restricted to mixtures at the eutectic point composition, nor are they even restricted to eutectic mixtures, which exhibit negative deviations from thermodynamic ideality.[32]

In this work, we examine dynamics in 1:3 molar ratio mixtures of tetraethylammonium (TEA) bromide (Br) or chloride (Cl) and ethylene glycol (EG) (1:3TEABr/EG and 1:3TEACl/EG) by using linear and ultrafast nonlinear infrared spectroscopies. Figure 1 shows the chemical structures of the TEA cation, the halide anions, and EG. It also shows space-filling structures of TEA^+, EG, and the anions, including the vibrational probe, selenium cyanate ($SeCN^-$). The space-fill structures have the approximately correct relative sizes. We use the CN stretch of the $SeCN^-$ vibrational probe to examine these DES from an anionic perspective.

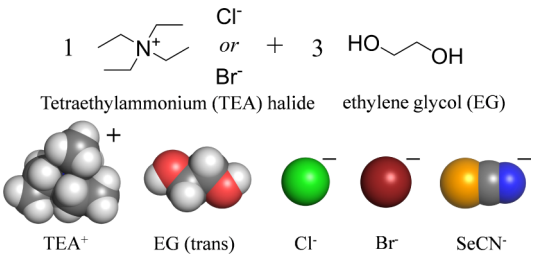

Figure 1. Chemical structures of the TEA cation, halide anions, and EG, along with their respective space-filling models.

The vibrational probe $SeCN^-$ encounters a more heterogeneous environment in pure EG compared with the tetraethylammonium halide/EG mixtures. The CN stretch linear absorption spectrum is substantially broader and double-peaked in pure EG, while it is narrower and has a single band when the probe is in the mixture. The probe spectra in TEABr and TEACl are virtually identical. However, the IR probe dynamics measured using IR nonlinear experiments, i.e., polarization-selective pump−probe (PSPP) experiments, exhibit significant differences. PSPP experiments were used to measure the probe's vibrational lifetimes and orientational relaxation dynamics.

The CN stretch lifetimes are almost the same in TEABr/EG and TEACl/EG, but they are a factor of 2 slower than in EG. Additionally, although the probes' spectra and lifetimes are virtually identical for TEABr/EG and TEACl/EG, their orientational relaxation dynamics differ. Observed multi-exponential orientational decays are caused by short time scale environmental restrictions that limit the range of angles to a cone of angles. Complete orientational randomization occurs on a longer time scale. In TEABr/EG and TEACl/EG, both the restricted angular sampling and the complete randomization differ.

Deep eutectic solvents are frequently discussed as mixtures with H-bond donors and H-bond acceptors, with a focus on the specific interactions among the components of the liquid. There is an additional way to think about DES such as 1:3 TEACl/EG and 1:3 TEABr/EG, which is in the context of our understanding of water-in-salt solutions. Water-in-salt solutions are aqueous salt solutions in which the concentration of salt is so high that there are far too few water molecules to solvate the ions. In low salt concentrations, an aqueous solution of LiCl will have Li^+ and Cl^- separated by water. Water is both an H-bond donor and an acceptor. When there is sufficient water, ∼4 water molecules solvate a Li^+ and 6−8 waters solvate a Cl^-.[33,34] The cations are solvated by water oxygens, and the anions are solvated by water hydroxyls.

At very high salt concentrations, in the water-in-salt regime, e.g., 1 ion pair per 4 water molecules (1:4), there are not nearly enough water molecules to fully solvate the ions. For a salt like LiCl, there are contact ion pairs, head-to-tail ion chains, and clusters of chains joined by solvent-separated ion pairs.[35] Consequently, the liquid exists as an extended ion/water network. The properties of water-in-salt solutions are very different from those of low-concentration saltwater solutions. For example, the water of a saltwater solution has an electrochemical window of 1.23 V.[36] However, in water-in-salt solutions, the electrochemical window is as high as 3 V.[37]

1:3 TEACl/EG and 1:3 TEABr/EG in many respects are analogous to LiCl and LiBr and other water-in-salt solutions. EG is both a H-bond donor and an acceptor. It can donate two

https://doi.org/10.1021/acs.jpcb.4c08739
J. Phys. Chem. B XXXX, XXX, XXX−XXX

H-bonds and accept two H-bonds. As with water-in-salt solutions, there are not nearly enough EGs to solvate TEA^+ and Cl^- or Br^-. While there are likely steric constraints, 3 EGs or more are required to provide 6 hydroxyls to solvate a halide anion. TEA^+ is a large quasi-spherical cation with a relatively low charge density, which can form many weak hydrogen bonds with EG.[38] Therefore, the mixtures are composed of ion pairs and large ion/EG clusters. A negligible number of ion pairs will be fully solvated and separated from other ions by the surrounding EGs. It is almost impossible for a single ion, TEA^+, or a halide to be solvent-separated from all other ions. Therefore, the mixtures should not be thought of as ions in an EG solvent but rather as a continuous network of ion/EG structures.

The orientational relaxation experimental results presented for 1:3 TEACl/EG and 1:3 TEABr/EG are compared to results from the literature for LiCl and LiBr 1:4 water-in-salt solutions. The values of the observables for the 1:3 TEACl/EG and 1:3 TEABr/EG systems differ markedly from those for LiCl and LiBr. However, some features of the ion/EG and ion/water results are very similar, suggesting that both types of systems have properties that reflect extended ion/solvent networks.

2. EXPERIMENTAL METHODS

2.1. Sample Preparation and Viscosity Measurements. Individual components of the eutectic mixtures include ethylene glycol (anhydrous, 99.8%, Sigma-Aldrich), tetraethylammonium chloride (BioUltra, ≥99.0%, Sigma-Aldrich), and tetraethylammonium bromide (ReagentPlus, 99%, Sigma-Aldrich). EG was placed in a nitrogen-filled glovebox and used as is. Tetraethylammonium chloride (TEACl) and tetraethylammonium bromide (TEABr) were dried under vacuum (∼60 mTorr) and heat (∼100 °C) for at least 15 h, and dryness was checked via FT-IR of the water hydroxyl stretch band.

A molar ratio of 3 parts EG to 1 part tetraethylammonium halide (TEAH) was prepared gravimetrically in the glovebox, and the mixture was stirred at ∼80 °C for 2 h following the recommended procedure of Gurkan et al. to ensure complete mixing.[39] This molar ratio was chosen to maximize the amount of TEAH present while ensuring complete solubility of the vibrational probe, KSeCN, at 0.05 M in the TEAH/EG mixture. As a control, several KSeCN concentrations above and below 0.05 M were tested to ensure that the probe concentration, especially the potassium cation, did not perturb the structure nor the dynamics of the liquid.[40] The spectra and dynamics are unaffected by probe concentrations up to at least 0.10 M of KSeCN.

The dynamic viscosity is measured by using the Rheosense model m-VROC-II with a B05 chip at ambient temperature (∼22 °C). The reported values for each sample are the average of five measurements.

2.2. Linear Infrared Spectroscopy. An FT-IR spectrometer with a spectral resolution of 0.5 cm^{-1} was used to collect the linear infrared spectra of the mixtures. The FT-IR spectrometer was purged with dry N_2 to minimize any absorption from gaseous CO_2 and H_2O. The TEAH/EG mixture was sandwiched between two CaF_2 windows that were 3 mm thick and 25 mm in diameter. A 56 μm Teflon spacer (Harrick Scientific) set the path length between the two windows. The TEAH/EG sample, CaF_2 windows, and anodized aluminum sample cell were assembled in a glovebox to prevent water vapor contamination. FT-IR spectra of TEAH/EG in the absence of KSeCN were used to perform background subtraction to isolate the nitrile stretch of the vibrational probe.

2.3. Nonlinear Infrared Spectroscopy. Ultrafast IR PSPP experiments were conducted as detailed in a previous publication.[41] A mode-locked Ti:sapphire oscillator seeds a chirped pulse regenerative amplifier to produce ∼100 fs pulses of 800 nm light at a 1 kHz repetition rate. A home-built optical parametric amplifier and difference frequency generator downconvert the 800 nm pulses into ∼6 μJ mid-IR pulses centered at 2068 cm^{-1} with a pulse duration of ∼170 fs and a bandwidth of ∼90 cm^{-1}. The mid-IR pulses are split by a ZnSe beam splitter into a strong pump path and a weak probe path. The pump pulses pass through a germanium acousto-optic pulse shaper to modulate the amplitude and phase of the pump pulses to reduce scattered light. The timing of the probe pulse is controlled relative to the pump pulse using a precision mechanical delay stage.

The probe pulse passed through the sample spatially overlapped with the pump pulse at a variable time delay of t after the pump pulse. The pump was polarized at 45° relative to the horizontally polarized (0°) probe pulse, and transient intensity differences in the probe were resolved at +45° and −45° to obtain parallel $S_{\parallel}(t)$ and perpendicular $S_{\perp}(t)$ signals, respectively. The frequency components of the signal are dispersed in a spectrograph and detected by a mercury cadmium telluride (MCT) array detector. A polarizer is placed immediately before the entrance slit of the spectrograph to project the $S_{\parallel}(t)$ and $S_{\perp}(t)$ signals onto the same horizontal (0°) polarization and adjusted to make the resulting parallel and perpendicular spectra identical in amplitude.

2.4. Density Functional Theory Calculations. Geometry optimizations of all structures were performed using the Gaussian 16 quantum chemistry package[42] at PBE/6-31 + G(d,p) level of theory with the SMD implicit solvent model.[43] For ethylene glycol, the custom implicit solvent is defined by using a dielectric constant of 37 and an optical dielectric constant of 2.045. Frequency and electrostatic potential (ESP) calculations are conducted at the same level of theory. All DFT works are performed on the Sherlock server at Stanford University.

3. RESULTS AND DISCUSSION

3.1. Linear Infrared Absorption Spectra. Background-subtracted linear absorption spectra of the CN stretch of $SeCN^-$ dissolved in 1:3TEACl/EG, 1:3TEABr/EG, and pure EG are plotted in Figure 2A. The spectra in TEACl/EG and TEABr/EG appear as single peaks. The spectrum in the EG has a shoulder on the blue side of the line. To determine the center frequencies and full width at half maxima (fwhm) of the nitrile vibrational bands in the mixtures, each peak was fit to a Gaussian line shape function between 2050 and 2130 cm^{-1}. Low-frequency tails of the spectra, caused by enhanced absorption (larger transition dipole) due to the vibrational non-Condon effect,[44,45] were excluded from the line shape fits. Quantitative results from the fits to the mixture spectra (Figure 2A) are reported in Table 1 and show minimal differences between 1:3TEACl/EG and 1:3TEABr/EG. The nitrile stretch is blue-shifted by 0.5 cm^{-1} in TEABr/EG (2067.8 cm^{-1}) and exhibits a ∼1 cm^{-1} broader full width at half-maximum (fwhm), 30.2 cm^{-1}, compared to $SeCN^-$ in TEACl/EG.

https://doi.org/10.1021/acs.jpcb.4c08739
J. Phys. Chem. B XXXX, XXX, XXX−XXX

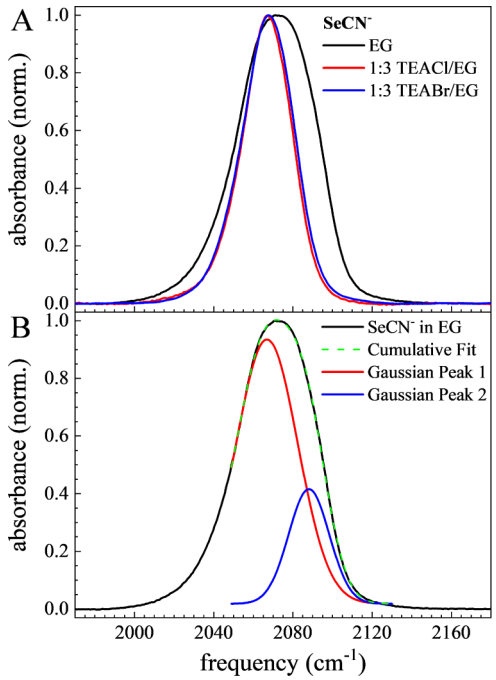

Figure 2. (A) FT-IR spectra of the $SeCN^-$ nitrile stretching mode in ethylene glycol (EG) and 1:3TEACl/Br-EG deep eutectic solvents. The EG spectrum is much broader and has two peaks. (B) Double Gaussian fit to the $SeCN^-$ spectra in EG. The lower frequency peak corresponds to the $SeCN^-$ bonded to EGs with gauche configurations, and the higher frequency peak is attributed to $SeCN^-$ bonded to EGs with trans configurations.

Table 1. Infrared Spectrum Center Frequencies and FWHM Values from Gaussian Fits to the Linear Absorption Spectrum and Vibrational Lifetimes of $SeCN^-$ in Ethylene Glycol (EG), 1:3Tetraethylammonium Bromide (1:3TEABr/EG), and 1:3Tetraethylammonium Chloride (1:3TEACl/EG)

Sample	Center (cm^{-1})	fwhm (cm^{-1})	Lifetime (ps)
1:3TEACl/EG	2067.3 ± 0.1	29.0 ± 0.1	72.2 ± 0.5
1:3TEABr/EG	2067.8 ± 0.1	30.2 ± 0.1	71.4 ± 0.3
EG (Peak 1)	2066.9 ± 0.3	36.7 ± 0.5	∼5−10
EG (Peak 2)	2088.1 ± 0.2	24.1 ± 0.4	37.6 ± 0.3

However, the main feature of these two spectra is that they are very close to identical.

In contrast to the mixtures, the line width of $SeCN^-$ dissolved in pure EG (Figure 2B) is significantly broader and the peak is shifted to the blue. In addition, the frequency range around the peak is rounded. Inspection of this spectrum shows that there is a shoulder on the blue side of the line. The $SeCN^-$/EG spectrum (Figure 2B, black curve) did not fit well to a single Gaussian function.

Two Gaussian functions were required to produce a representation of the broad absorption feature. The two Gaussian fit curves are colored red and blue, and their sum is the green dashed curve, which reproduces the experimental spectrum (black curve) essentially perfectly. The two peaks shown in the fit of Figure 2B demonstrate that two significant subensembles of $SeCN^-$ are present in pure EG. One of the Gaussian bands obtained from the fits has virtually the same center frequency as those of the mixtures (2067 cm^{-1}), and the second band center is shifted to the blue, 2088 cm^{-1} (Table 1).

Cui et al. also observed a significantly broader line shape with a shoulder on the high frequency of the band of the CN stretch of SCN^- in ethylene glycol.[14] The blue shoulder decreased in intensity with the addition of choline ((2-hydroxyethyl)-trimethylammonium) chloride, a quaternary ammonium.[14] These results indicate that the addition of a quaternary ammonium cation modifies the pure EG H-bond network.

Figure 3 displays the results of DFT electronic structure calculations for a $SeCN^-$ bonded to an EG in gauche and trans

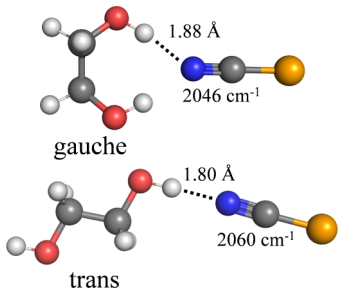

Figure 3. DFT-optimized structures for $SeCN^-$ bonded to EG. The gauche configuration is shown on the top, which has a calculated CN stretch frequency of 2046 cm^{-1}; the trans configuration is shown on the bottom with a frequency of 2060 cm^{-1}.

configurations at the PBE/6-31G+ (d,p) level of theory with the EG implicit solvent. Detailed MD simulations of $SeCN^-$ in water[37] show that the strongest H-bonds are hydroxyls associating with the N lone pairs along the axis of the molecule. A stronger hydrogen bond results in a blue shift. However, multiple additional H-bonds can be made off-axis. The electronic structure calculations show on-axis and off-axis H-bonding to the N lone pair. The H-bonding in the gauche and trans configurations gives CN vibrational frequencies of 2045.6 and 2059.5 cm^{-1}, respectively. These results are in good agreement with the experimental numbers of 2068 and 2088 cm^{-1} for the two peaks obtained from the fit in Figure 2B, given that the calculations use an implicit solvent rather than accounting for the molecular-level intermolecular interactions arising from the solvent environment. From the calculations, we can conclude that in pure EG, the blue band arises from on-axis H-bonding to EG in its trans configuration and the red band arises from off-axis H-bonding to EG in its gauche form.

The area of the red band in Figure 2B is approximately three times larger than that of the blue band. Stronger on-axis H-bonding decreases the transition dipole somewhat, so that a quantitative comparison of the peak areas is not possible. Nonetheless, the significantly larger area of the red band indicates that the gauche configuration is substantially more probable than the trans configuration that produces the blue band.

For the mixtures, both TEA^+ and EG can solvate $SeCN^-$ by forming H-bonds.[14,18,21] The EG hydroxyls, in both the trans and gauche forms, can make strong H-bonds to $SeCN^-$, with the trans conformation making stronger H-bonds. TEA methyl and methylene hydrogens have partial charges (ESP) of ∼+0.1, while the EG hydroxyl hydrogens have partial charges close to +0.5. Therefore, EG should form H-bonds stronger than those of TEA to $SeCN^-$, Cl^-, and Br^-. The $SeCN^-$s in the network will occupy anion sites that are likely similar to those populated by Cl^- or Br^-. The narrower inhomogeneous lines in the

https://doi.org/10.1021/acs.jpcb.4c08739
J. Phys. Chem. B XXXX, XXX, XXX−XXX

mixtures imply that $SeCN^-$ is interacting with a smaller variety of structures or the strengths of the interactions are weaker.

Although the line width of the red CN band in EG is slightly broader than the mixture bands, their center positions are virtually identical. This is strong evidence that in the mixtures, $SeCN^-$ is H-bonded to the gauche form of EG. In addition, it suggests that the incidence of the trans configuration is rare in the mixtures. The absence of the trans configuration is probably caused by the structure of the ion/EG network. The gauche form of EG must have more efficacy in solvating both anions and cations in structural environments that have contact ion pairs and solvent-separated ion pairs. Below, the DFT calculation will show that Cl^- and Br^- can bond to the gauche form of EG in the same manner as $SeCN^-$.

3.2. Isotropic Pump−Probe Decays. The vibrational lifetime of the $SeCN^-$ nitrile vibrational stretch was determined through isotropic pump−probe decays, $P(t)$

$$P(t) = \frac{S_{\parallel}(t) + 2S_{\perp}(t)}{3} \quad (1)$$

in which the $S_{\parallel}(t)$ and $S_{\perp}(t)$ are the parallel and perpendicular signals, respectively.[46−48] The isotropic decays of $SeCN^-$ in 1:3TEACl/EG and 1:3TEABr/EG mixtures are best suited to triexponential decays. Ten frequencies centered around the peak of the absorption band between 2062.8 and 2073.3 cm^{-1} were included in each fit. Due to the lack of frequency dependence observed in all three time constants, the time constant was shared across all ten frequencies during fitting. Figure 4 displays the isotropic decays at the center frequency for EG, 1:3TEABr/EG, and 1:3TEACl/EG with their respective triexponential fits to the data.

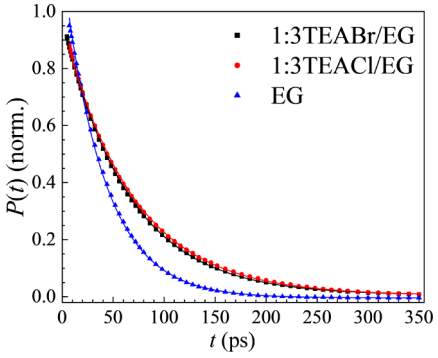

Figure 4. Isotropic pump−probe signals for EG, 1:3TEABr/EG, and 1:3TEACl/EG. The experimental data are fit to triexponential decays. The first two exponential decays result from spectral diffusion, and the third decay is the vibrational lifetimes. The vibrational lifetimes of $SeCN^-$ are almost identical in 1:3TEABr/EG and 1:3TEACl/EG, both of which are longer than the lifetime in EG.

The first two isotropic decay time constants are caused by spectral diffusion.[44,45] Amplitudes of the short isotropic decays are negative on the blue side of the band, which is observed as signal growth at early times. These observations are in accord with the non-Condon effect manifested in the FT-IR spectra on the red side wing. The pump pulse is absorbed more strongly on the red side of the absorption spectra because of the increased transition dipole moment. This nonuniform pumping of the $SeCN^-$ absorption band leads to an initial nonequilibrium frequency distribution of excited states followed by equilibration of the population across the inhomogeneously broadened absorption spectrum via spectral diffusion.[44,45]

The longest time constants of the triexponential isotropic decays are the vibrational lifetimes of $SeCN^-$ in TEACl/EG and TEABr/EG. The vibrational lifetimes of the CN stretch of $SeCN^-$ in these two liquids are 71.4 ± 0.3 and 72.2 ± 0.5 ps, respectively (Table 1). Vibrational relaxation of the initially excited CN stretch occurs by transferring vibrational energy to intramolecular and intermolecular modes.[49] The intramolecular pathways should be virtually the same in the two liquids. Stronger intermolecular interactions between the vibrational probe and its surrounding solvent can facilitate vibrational relaxation because it is necessary to deposit some energy into solvent bath modes in the decay of the initially excited vibration to conserve energy.[48−52] Since the lifetimes are on the edge of being within experimental error, the solvent environments around the probes are almost the same.

For $SeCN^-$ in pure EG, precise determination of the vibrational lifetimes is exceedingly challenging due to the extent of spectral overlap in the nitrile absorption (Figure 2B). Given the evidence of two spectral peaks from the linear spectrum, there should be two lifetimes. Analysis of $SeCN^-$ vibrational relaxation in EG is further complicated by overlapping $\nu = 0 \rightarrow 1$ and $\nu = 1 \rightarrow 2$ transitions on the low-frequency side of the spectrum. While the $\nu = 1 \rightarrow 2$ band is not observable in the linear FT-IR spectrum, it is present as a negative-going band in the nonlinear spectra. The higher frequency region of the $\nu = 0 \rightarrow 1$ transition is free from overlap with that of the $\nu = 1 \rightarrow 2$ transition. Hence, population decays between 2084.2 and 2086.7 cm^{-1} were analyzed to characterize vibrational relaxation. This region of the spectrum has almost equal contributions from the two absorption bands in Figure 2B.

Population decays of $SeCN^-$ nitrile stretching modes in EG (Figure 4) are fit to triexponential functions, and the time constants did not vary across the three frequencies included in the fits. Similar to the discussion for the mixtures, the first two time constants are attributed to spectral diffusion,[45] and the third time constant, t_3 = 37.6 ps, is the lifetime.

The important message here is that the decay in pure EG is approximately a factor of 2 faster than the lifetimes in the mixtures, suggesting that adding TEACl/Br to EG induces a significant change in solvent environments. This large difference is most likely caused by differences in the intermolecular continuum bath modes and their density of states in EG compared with the mixtures. Cui et al. and Chatterjee et al. observed faster vibrational relaxation of SCN^- and MeSCN nitrile stretches in EG compared to EG and choline chloride mixtures, respectively.[14,53]

3.3. Orientational Relaxation. Polarization-selective pump−probe decays also provide information on $SeCN^-$ orientational relaxation dynamics in ethylene glycol and the mixtures with the tetraethylammonium halide salts. Orientational anisotropy, $r(t)$, is obtained from PSPP experiments using

$$r(t) = \frac{S_{\parallel}(t) - S_{\perp}(t)}{S_{\parallel}(t) + 2S_{\perp}(t)} = 0.4C_2(t) \quad (2)$$

in which $C_2(t)$ is the second-order Legendre polynomial orientational correlation function.[46,47] The anisotropy decays at three frequencies on the blue side of the line for $SeCN^-$ in pure EG are plotted in Figure 5. $r(t)$ = 0.4 at t = 0 ps.

https://doi.org/10.1021/acs.jpcb.4c08739
J. Phys. Chem. B XXXX, XXX, XXX−XXX

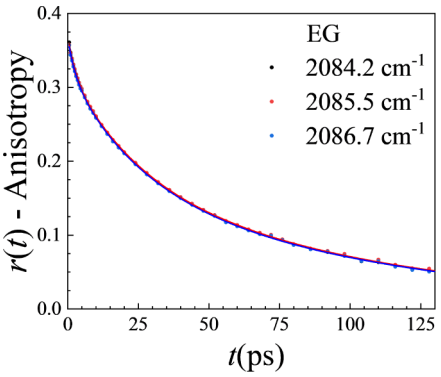

Figure 5. Anisotropy decay of $SeCN^-$ in EG. The $r(t)$s at three frequencies on the blue side of the absorption line overlap almost perfectly, showing a lack of frequency dependence. The data are fit to triexponential decays.

However, the anisotropy decays plotted in Figures 5 and 6 do not begin at $r(t) = 0.4$ because of the finite pulse duration used

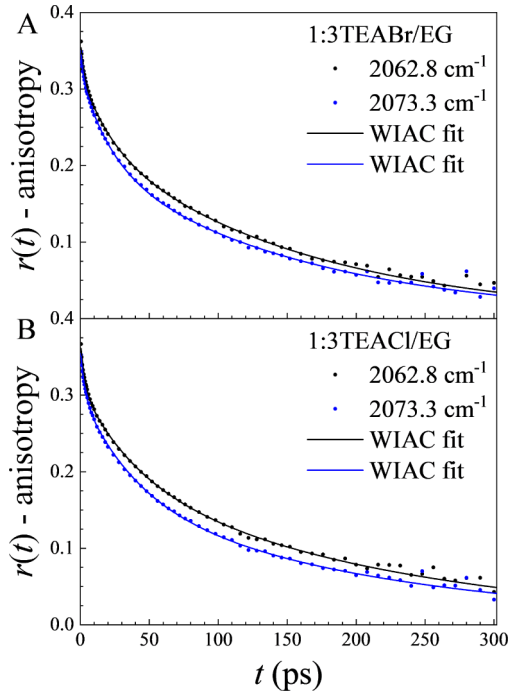

Figure 6. Anisotropy decays of $SeCN^-$ in the mixtures of the two tetraethylammonium halide salts with EG. The $r(t)$s are plotted at two absorption frequencies, which shows clear frequency dependence in both deep eutectic mixtures.

in the experiments, which obscures tens of femtosecond inertial angular motions.[54] The difference between the data extrapolated to $t = 0$ and 0.4 gives the amplitude of the inertial component, but the time constant cannot be determined.

The anisotropy decays of the probe in EG are described by triexponential functions. Here, only three frequencies on the blue side of the absorption spectrum (2084.2−2086.7 cm^{-1}) were included in the fits because of the spectral overlap of the $v = 0 \rightarrow 1$ and $v = 1 \rightarrow 2$ transitions at lower frequencies. Within this spectral range, the triexponential fits are frequency-independent in both time and amplitude. As a result, the amplitudes and time constants for the EG anisotropy decays were averaged across the three frequencies for further analysis.

In comparison, the $r(t)$ in TEABr/EG and TEACl/EG mixtures are wavelength-dependent (Figure 6). They were also fit to triexponential decays over ten frequencies around the peak centers, between 2062.8 and 2073.3 cm^{-1}. Here, only the two frequencies at each end of the measured spectral range are shown. Time constants differed negligibly across the absorption band; therefore, the time constants were shared across all frequencies, and the amplitudes were allowed to float.

The first two time constants are the same within error for $SeCN^-$ in pure EG and in TEABr/EG. The time constants are $t_1 = 2.3 \pm 0.3$ and $t_2 = 27 \pm 8$ ps for pure EG and $t_1 = 2.2 \pm 0.7$ and $t_2 = 27 \pm 6$ ps for 1:3TEABr/EG (Table 2). $SeCN^-$ in

Table 2. Wobbling-in-a-Cone Time Constants for Restricted Orientational Diffusion for $SeCN^-$ in EG, 1:3TEABr/EG, and 1:3TEACl/EG

Sample	τ_{c1} (ps)	τ_{c2} (ps)	τ_m (ps)	Viscosity (mPa·s)
EG	2.3 ± 0.3	27 ± 8	94 ± 9	16.95 ± 0.03
1:3TEACl/EG	3.1 ± 0.2	49 ± 4	215 ± 22	30.91 ± 0.10
1:3TEABr/EG	2.2 ± 0.7	27 ± 6	161 ± 12	29.13 ± 0.04

TEACl/EG exhibits slower anisotropy decay constants compared to pure EG and TEABr/EG: $t_1 = 3.1 \pm 0.2$ ps and $t_2 = 49 \pm 4$ ps. The third time constant for complete orientational relaxation differs significantly among all three liquids; the third orientational relaxation time constants are 94 ± 9 ps (EG), 161 ± 12 ps (TEABr/EG), and 215 ± 22 ps (TEACl/EG). The time constants and decay amplitudes will be discussed further in the context of the wobbling-in-a-cone (WIAC) model.

The simplest type of orientational relaxation, small-step Gaussian diffusion, can be analyzed using the Stokes−Einstein−Debye (SED) equation and its extensions.[55,56] This type of orientational relaxation gives rise to a single exponential decay of the experimental anisotropy; i.e., $C_2(t)$ (eq 2) decays as a single exponential. In the context of the SED equation, the single exponential decay constant, t, is related to the orientational diffusion constant, D, by

$$\tau = \frac{1}{6D} \tag{3}$$

However, all of the anisotropy decays for the three liquids studied are triexponential. Biexponential and triexponential orientational relaxation decays are frequently observed for probe molecules in complex liquids. To quantify $SeCN^-$'s orientational relaxation, the anisotropy data were fit to the WIAC model.[57−60] In this model, $SeCN^-$ reorients in a series of angular cones that limit the extent of angular rotation followed by complete orientational randomization. The initial cone is caused by nondiffusive ultrafast inertial motions with a cone half angle of θ_I. This is followed by the first diffusive cone, with a cone half angle of θ_{c1}. θ_I and θ_{c1} are sampled before the structural evolution of the local liquid environments permits an increased angular range to be explored. The range sampled prior to structural relaxation is θ_{fast}, the combination of ranges sampled by θ_I and θ_{c1}. As time increases, structural evolution relaxes the solvation configurations that confine the probe orientational relaxation to the first cone, increasing the sampled angular range to the second cone, θ_{c2}. Further structural evolution relaxes confinement and the probe orientation randomizes.

https://doi.org/10.1021/acs.jpcb.4c08739
J. Phys. Chem. B XXXX, XXX, XXX−XXX

Table 3. Wobbling-in-a-Cone Parameters for $SeCN^-$ in 1:3TEABr/EG and1:3TEACl/EG at Line Center, 2067.4 cm^{-1}, and the Parameters for Pure EG

Sample	θ_I (deg)	θ_{c1} (deg)	θ_{fast} (deg)	θ_{c2} (deg)	θ_{tot} (deg)	$(6D_{c1})^{-1}$ (ps)	$(6D_{c2})^{-1}$ (ps)	$(6D_m)^{-1}$ (ps)
EG	13 ± 1	16 ± 1	20 ± 1	32 ± 6	38 ± 5	19 ± 2	54 ± 9	94 ± 9
1:3TEACl/EG	14 ± 2	15 ± 2	21 ± 2	27 ± 2	34 ± 2	19 ± 2	73 ± 9	161 ± 12
1:3TEABr/EG	14 ± 2	18 ± 2	23 ± 2	33 ± 2	39 ± 2	18 ± 3	95 ± 6	215 ± 22

The orientational correlation function for the WIAC model comprises ultrafast inertial motions, restricted angular diffusion, and finally complete diffusive orientational randomization:[57]

$$C_2(t) = T^2(S^2 + (1 - S^2)e^{-t/\tau_{c1}})(R^2 + (1 - R^2)e^{-t/\tau_{c2}}) e^{-t/\tau_m} \quad (4)$$

The generalized order parameter T^2 reflects the inertial motions. There is no time constant associated with T^2 because the inertial decay is too fast to measure. Because the orientational relaxations of all samples at all wavelengths are triexponential decays, there are two WIAC diffusion processes described by the order parameter S^2 and the wobbling time constant τ_{c1} for faster wobbling diffusion and by R^2 and τ_{c2} for slower $SeCN^-$ restricted diffusive motion. Finally, unrestricted orientational diffusion occurs with the time constant τ_m.[61] The cone half angles, θ_c, can be extracted from the squared order parameters: T^2, S^2, and R^2.[59]

$$Q^2 = \left[\frac{1}{2}\cos\theta_c(1 - \cos\theta_c)\right]^2 \quad (5)$$

In addition to the individual cone angles, θ_I, θ_{c1}, and θ_{c2}, the entire restricted angular space available is given by the combination of the three cones,the total cone (θ_{tot}), which can be calculated from the total order parameter $Q_{tot} = TRS$. The cone angle sampled before solvent rearrangements, θ_{fast}, is given by $Q_{fast} = TS$.[62] The time constants τ_{c1}, τ_{c2}, and τ_m are related to the triexponential fit time constants to the anisotropy decays by,[61]

$$\tau_{c1} = t_1, \quad \tau_{c2} = (1/t_2 - 1/t_3)^{-1}, \quad \text{and} \quad \tau_m = t_3 \quad (6)$$

The orientational diffusion coefficients for the unrestricted orientational relaxation were calculated directly from τ_m using the Debye model given in eq 3. However, the cone diffusion constants depend on both the cone decay time constant and the cone half-angle. Wobbling diffusion constants D_{c1} and D_{c2} were obtained from the following expression:[59]

$$D_c = \frac{\cos^2(1 + \cos\theta_c)^2\{\ln[1 + \cos\theta_c/2] + (1 - \cos\theta_c)/2\}}{\tau_c(1 - Q^2)[2(\cos\theta_c - 1)]} + \frac{(1 - \cos\theta_c)(6 + 8\cos\theta_c - \cos^2\theta_c - 12\cos^3\theta_c - 7\cos^4\theta_c)}{24\tau_c(1 - Q^2)} \quad (7)$$

Wobbling-in-a-cone analysis for restricted orientational diffusion provides information about the solvent environments experienced by the vibrational probe in the DES. For complete orientational relaxation (eq 3), the time constant (τ_m) is related to the diffusion constant by $(6D_m)^{-1}$. We use this same form to obtain the wobbling orientational relaxation times from the diffusion constants. Table 3 gives the cone angles for EG, 1:3TEABr/EG, and 1:3TEACl/EG. Because the cone angles are wavelength-dependent for the mixtures, the values are given at the line center: 2067.4 cm^{-1}. The EG orientational relaxation parameters are not frequency-dependent (Figure 5).

We are primarily interested in examining the effects of the anions on the mixtures, but first, it is worthwhile to compare the mixtures' orientational relaxation properties to those of EG. θ_{fast} is the cone half-angle for motions on time scales on which the probe sees a distribution of local environments that have not evolved. From Table 3, the cone half-angle of the inertial cone, θ_I, the first diffusive cone, θ_{c1}, and their combination, θ_{fast}, are all the same within experimental error. Because of the large error bars, the value of θ_{c2} for EG overlaps with those of the mixtures, but the θ_{c2} values for the mixtures show statistically significant differences. Additionally, the θ_{c2}s for the mixtures are frequency-dependent, while θ_{fast} does not have this attribute. The frequency-dependent cone angles are characteristics of an extended ion/solvent network,[63] as discussed in Section 3.4 during the comparison to water-in-salt electrolytes.

It is instructive to compare the complete orientation times (τ_m) of $SeCN^-$ in 1:3TEACl/EG and 1:3TEABr/EG. While the wobbling correlation times are the same within error for the three liquids, τ_m reveals some interesting differences. Their τ_ms are 215 and 161 ps, respectively. 1:3TEACl/EG has a very similar viscosity to 1:3TEABr/EG, 30.9 vs 29.1, which is a ratio of 1.06. The ratio of the orientational relaxation times is 1.34, much larger than the increase in viscosity. Therefore, the slower complete reorientation time for TEACl/EG is likely a result of increased interaction within the surrounding environments that are not reflected in the bulk viscosity. It is possible that the increased interaction caused by the higher charge density of Cl^- compared to Br^- is more prominent near the halide anions or the anion probe $SeCN^-$ due to the increased local charged interactions, while other regions of the extended network are not affected as much. Therefore, the average over the entire system (bulk viscosity) displays a smaller difference. This disparity between the orientational relaxation time ratio and bulk viscosity ratio suggests the existence of dynamic heterogeneity within deep eutectic solvent systems. Such heterogeneity is not surprising given the complexity of the molecular-level structures. This proposition is further examined below, with more information from DFT calculations.

In the highly concentrated mixtures studied here, with a ratio of 1:3, there are not nearly enough EGs to solvate the cations and anions, including $SeCN^-$. There will be contact ion pairs and solvent-separated ion pairs that form continuous ion/EG networks. As discussed, these concentrated ion/EG mixtures are analogous to highly concentrated aqueous salt solutions, i.e., water-in-salt solutions. In solutions such as LiCl and LiBr, water can donate two H-bonds and accept two H-bonds. In 1:3TEACl/EG and 1:3TEABr/EG, the TEA cations and the solvating neutral molecules, EG, are very different from Li^+ and H_2O. However, like H_2O, EG can donate two H-bonds and accept two H-bonds. The FT-IR spectrum of $SeCN^-$ in the mixtures and the DFT calculations show that the EG exists in the gauche form when the probe is solvated (Figure 3).

https://doi.org/10.1021/acs.jpcb.4c08739
J. Phys. Chem. B XXXX, XXX, XXX−XXX

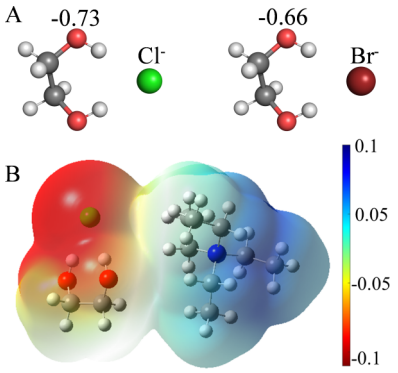

Figure 7. (A) DFT calculation of EG H-bonded to Cl^- and Br^- and the partial charges on EG oxygens. When EG is bonded to a Cl^-, the partial negative charges on the EG oxygens are larger than when EG is bonded to Br^-. (B) DFT-optimized structure of the EG−Cl^- cluster interacting with TEA^+, along with the associated electrostatic potential map.

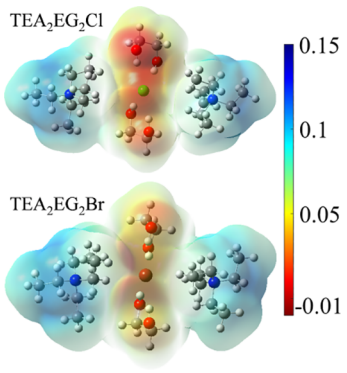

Figure 8. DFT-calculated illustrations of possible TEA^+-EG/anion network structures. Here, Cl^- (top) and Br^- (bottom) are complexed to two EGs to form a cluster, which can interact weakly with TEA^+ on both sides, forming a sandwiched structure. The contours show the electrostatic potential map of the cluster, which suggests higher density around Cl^- than Br^-.

Figure 7A shows a DFT calculation of EG H-bonded to Cl^- and Br^- as well as the partial charges on EG oxygens. In this configuration, the two oxygen lone pairs are available to solvate TEA cations. From DFT calculations, the partial charges on the TEA^+ hydrogens are small, ∼0.1; therefore, H-bonds to these cations will be relatively weak. However, the EG/anion complexes can interact with a number of TEA hydrogens. Because H-bonds to TEA^+ are weak, the ion/EG network is highly dynamic. Complexes can shift on the TEA^+ "surface" among different sets of hydrogens and switch between TEA^+s. The network dynamics will give rise to wobbling and complete orientational randomization of the probe.

DFT calculations of the EG/anion structure shown in Figures 7A and 3 (gauche configuration) show that EG/Cl^- H-bonding is slightly weaker than EG/$SeCN^-$, 8.7 kcal/mol vs 8.8 kcal/mol. The EG/Br^- H-bonding is considerably stronger at 14.7 kcal/mol. These interactions correspond to ∼15 k_BT and ∼26 k_BT at room temperature. Both are so large relative to k_BT that the EG/anion complexes should remain intact on the time scale of orientational relaxation. While these values do not consider other intermolecular interactions, the anion−EG interactions are so large that it is unlikely they will be reduced to values of a few k_BT.

Consider a simple qualitative scenario to explain the faster orientational relaxation in the Br^- mixture compared to that in the Cl^- mixture. DFT calculations show that the EG-solvated anions have three non-negligible interactions with TEA^+s. Figure 7B is the result of a DFT calculation for one configuration with an associated electrostatic potential map. The interactions are weak because of the small partial positive charges, ∼0.1, on the TEA^+ hydrogens. Multiple EG/anion complexes will solvate a TEA^+, and the complexes can interact with two TEA^+s, weakly coupling pairs. The bridging of two TEA^+s by EG/ion complexes is simultaneously contact ion pairs and solvent-separated ion pairs as both the anions and the EGs can concurrently bind to and form a "sandwich" with a pair of TEA^+s. DFT-calculated illustrations of a pair of TEA^+s complexed by two EG/halide complexes (Cl^- and Br^-) are shown in Figure 8. Structures like the ones shown in Figure 8 extend in three dimensions. The result will be a TEA^+-EG/anion network.

However, because EG/anion complexes interact weakly with TEA^+, there will be continuous changes in structure. Through restricting interactions, the motions of the complexes will be tied to each other. On a short time scale, the complexes can wobble about particular local configurations. For the complexes that contain $SeCN^-$, the result is partial orientational relaxation, i.e., wobbling-in-a-cone. Motions of the TEA^+s and EG/anion complexes will produce larger shifts and change the particular TEA^+s to which EG/anion is bonded, resulting in complete orientational randomization of the EG/$SeCN^-$ complexes. For TEACl/EG, the higher charge density on Cl^- can more effectively pull electrons from EG, resulting in larger partial negative charges on the EG oxygens compared to Br^--bonded EG (Figure 7A). Therefore, the interactions between the EG anion pair and TEA^+ will be stronger in TEACl/EG than in TEABr/EG. The rates of orientational randomization of the probe complex EG/$SeCN^-$ are also consistent with such an interpretation. Initially, the probe complex (Figure 3, gauche) will be wobbling in an essentially fixed local environment. The values of $(6D_{c1})^{-1}$ for the two halide mixtures are the same within experimental error (Table 3). However, both $(6D_{c2})^{-1}$ and $(6D_m)^{-1}$ are faster for the Br^- mixture than for the Cl^- mixture. Since these two processes require the probe's surrounding environment to undergo structural relaxation, the orientational diffusion rate will be faster for the system with the weaker hydrogen bonding network (Br^-).

3.4. Comparison to Water-in-Salt Electrolytes.

1:3TEACl/EG and 1:3TEABr/EG solutions and 1:4LiCl and 1:4LiBr aqueous solutions both form extended networks of ions and neutral molecules. Similar PSPP studies have been reported for the two lithium/halide systems.[63] The OD stretch of dilute HOD in H_2O was used as the vibrational probe of the lithium/halide aqueous solutions to measure the orientational relaxation characteristics. The OD lifetimes and orientational relaxation times are much faster in the lithium halide/H_2O solutions than in the TEA halide/EG solutions, and the OD stretch absorbs at ∼4 μm, while the CN stretch absorbs at ∼5 μm. Although the two types of systems are very different, there are two interesting comparisons that can be made, which may shed light on the common characteristics of an extended hydrogen bonding network.

The first comparison is the change in the complete orientational randomization times, τ_m, when the halide is changed. As discussed above, for 1:3TEACl/EG and

https://doi.org/10.1021/acs.jpcb.4c08739
J. Phys. Chem. B XXXX, XXX, XXX−XXX

1:3TEABr/EG mixtures, the τ_ms are 215 and 161 ps, with a ratio of 1.34 ± 0.1. For 1:4LiCl and 1:4LiBr aqueous solutions, the τ_ms are 12 and 9 ps, with a ratio of 1.33 ± 0.1. Both systems have far too few solvent molecules to solvate the ions fully, which means there are contact ion pairs and solvent-separated ion pairs, giving rise to extended ion/EG networks. In both systems, the Cl^- solutions have a slower orientational relaxation than their Br^- counterparts, and the ratios of the relaxation times are the same within experimental error. This similarity in the ratios may be a coincidence or the result of the influence of a larger halide (lower charge density) on the dynamics of ion/solvent extended networks. Figure 9 shows

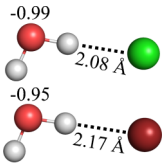

Figure 9. DFT calculation of water molecules H-bonded to Cl^- (top) and Br^- (bottom) as well as the partial charges on the water oxygens. Like ethylene glycols, the partial negative charge on water oxygen is larger when it is bonded to Cl^- than Br^-.

DFT-optimized structures of water molecules bonded to Cl^-/Br^- along with the partial charges on the oxygens. Similar to the case of EG bonded to a Cl^-/Br^- (Figure 7A), the negative charge on oxygen is larger when bonded to Cl^- compared to Br^-, resulting in a stronger hydrogen bonding network. Below, frequency-dependent cone angles also show that the two types of systems behave nearly identically.

As discussed above, the $SeCN^-$ orientational relaxation consists of sampling a limited range of angles, the cone of angles, at short times followed by complete orientational randomization. The first two cone angles are wavelength-independent for the 1:3TEACl/EG and 1:3TEABr/EG solutions. However, the final cone angle before complete orientational relaxation, θ_{c2}, depends on the wavelength. Figure 10A shows the dependence of the cone angle on the frequency for wavelengths around the line center. The cone angles are plotted against the difference in the frequency from the line center in terms of the standard deviation of the line width. Δ stn. div. is the fraction of a standard deviation from the line center. Making the plot this way allows the results from samples with different center wavelengths and line widths to be compared. The cone angles get larger as the frequency increases, i.e., going from negative Δ stn. div. to positive Δ stn. div.

The size of the available volume around the vibrational probe determines the cone angle. The available volume, which has a distribution of sizes, gives rise to different cone angles. Wavelength-dependent cone angles occur if the probes' local environments exist for times long compared to the cone sampling time and if the absorption frequency is correlated with the size of the volume. A detailed study has been presented on the relationship between cone angles and frequency that involves first-order Stark coupling to the medium.[64] A smaller volume is associated with a stronger local E-field, which causes the observed frequency to red-shift. Here, the observed cone angles decrease as the frequency shifts to the red side, consistent with a previous interpretation.

Figure 10B shows the frequency-dependent cone angles again for the cone before complete randomization for 1:4LiCl/H_2O and 1:4LiBr/H_2O. The values were obtained from the literature.[63] The 1:3TEACl/EG and 1:3TEABr/EG mixtures' absorptions are centered near 5 μm and have line width fwhm's of ~30 cm^{-1}. The 1:4LiCl/H_2O and 1:4LiBr/H_2O mixtures' absorptions are centered near 4 μm and have fwhm's of ~160 cm^{-1}. Nonetheless, the data were plotted in terms of Δ stn. div., so the changes in going from Cl^- to Br^- can be compared. Both systems show a clear increase in cone angle with blue-shifted frequency with bromide salts having larger cone angles at all frequencies. Additionally, the ratio of the cone angles (Br^-/Cl^-) can be compared for the two systems at their respective line centers. The ratio is 1.16 ± 0.05 for the TEA^+/EG systems and 1.09 ± 0.06 for the Li^+/H_2O systems, which are the same within error. The fact that going from chloride to bromide anions produces the same fractional increase within error in ethylene glycol deep eutectic solvents and in water-in-salt electrolytes shows a second common characteristic of the two types of ion-neutral molecule extended network systems.

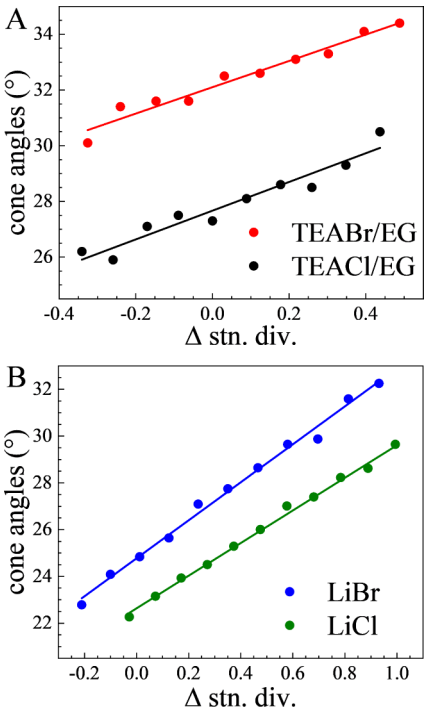

Figure 10. Frequency-dependent cone angles for (A) TEA halide/EG deep eutectic solvents and (B) lithium halide/H_2O Water-in-Salt electrolytes. The frequencies are plotted as the standard deviations around the respective absorption line centers to easily compare the systems.

4. CONCLUDING REMARKS

Ultrafast polarization-selective pump−probe (PSPP) experiments were presented for pure ethylene glycol (EG) and 1:3TEACl/EG and 1:3TEABr/EG mixtures (1:3—one ion pair per 3 EGs). The anionic vibrational probe $SeCN^-$ was used to investigate the properties of the three liquids. The $SeCN^-$ CN stretch displayed two peaks in EG but only one peak in the 1:3TEACl/EG and 1:3TEABr/EG mixtures. DFT calculations showed that the two vibrational frequencies of the CN stretch in EG were consistent with the $SeCN^-$ anion H-bonding to EG in its trans and gauche configurations (Figure 3). However, in the mixtures, the single peaks in the CN spectra (Figure 2) and DFT calculations (Figure 7A) showed

https://doi.org/10.1021/acs.jpcb.4c08739
J. Phys. Chem. B XXXX, XXX, XXX−XXX

that EG H-bonds to all three anions, Cl^-, Br^-, and $SeCN^-$, only in its gauche configuration.

Using PSPP, the orientational relaxation of the probe was measured in the two TEA/halide mixtures and EG (Tables 2 and 3). The mixtures displayed multiexponential decays. The two fast components arise from partial orientational sampling of a limited range of angles, cones of angles, followed by the slowest component, the time constant for complete orientational randomization. Although 1:3TEACl/EG and 1:3TEABr/EG mixtures have almost the same viscosities, the complete orientational randomization of 1:3TEABr/EG is significantly faster than that of 1:3TEACl/EG (Table 2). The cone angle prior to complete orientational randomization was found to be wavelength-dependent (Figure 9A). The cone angles vs frequency for the two mixtures fall on lines, with the Br^- system having larger cone angles than Cl^- across all frequencies.

It was suggested that 1:3TEACl/EG and 1:3TEABr/EG mixtures should not simply be considered solutions of ions dissolved in a neutral solvent. For a ratio of one ion pair per three EGs, there are not nearly enough EGs to solvate the cations and anions. There will be contact ion pairs and solvent-separated ion pairs at this very high ion concentration. The liquids will exist as an extended network of these ion pairs. The deep eutectic solvents investigated in this study are analogous to water-in-salt solutions, which are extremely highly concentrated salt solutions with far too few water molecules to solvate the salt anions and cations, e.g., 1:4LiCl/H_2O and 1:4LiBr/H_2O. Water-in-salt solutions form extended ion/water networks. Some possible clusters that would continue in three dimensions and form the extended 1:3TEACl/EG and 1:3TEABr/EG networks were obtained from DFT calculations (Figures 7 and 8).

PSPP data for 1:4LiCl/H_2O and 1:4LiBr/H_2O from the literature[63] show remarkable similarities to the mixtures studied here. The ratio of the complete orientational relaxation times, τ_m, for 1:3TEACl/EG and 1:3TEABr/EG is 1.33. The 1:3 TEA halide/EG deep eutectic mixtures and 1:4 lithium halide/H_2O water-in-salt electrolytes are very different. TEA^+ is much larger than Li^+, and EG is much larger than water. The TEA halide solutions have viscosities substantially higher than those of the 1:4LiCl/H_2O and 1:4LiBr/H_2O solutions. Nonetheless, the ratio of the complete orientational relaxation times for 1:4LiCl/H_2O and 1:4LiBr/H_2O is identical to that of deep eutectic solvents within error. In addition, at the line centers, the ratio of the orientational cone angles of the TEABr and TEACl systems is the same within error as the ratio of the LiBr and LiCl systems.

Correlation is not causation, but the correlations are interesting. Br^- is larger and has a charge density lower than that of Cl^-, giving rise to a "looser" network. The results suggest that this effect is responsible for the observed changes in switching from Cl^- to Br^- in these two very different types of extended ion/neutral molecule networks.

AUTHOR INFORMATION

Corresponding Author

Michael D. Fayer − *Department of Chemistry, Stanford University, Stanford, California 94305, United States;* orcid.org/0000-0002-0021-1815; Phone: +(650) 723-4446; Email: fayer@stanford.edu

Authors

Junkun Pan − *Department of Chemistry, Stanford University, Stanford, California 94305, United States;* orcid.org/0000-0001-6128-1844

Kimberly A. Carter-Fenk − *Department of Chemistry, Stanford University, Stanford, California 94305, United States; Department of Chemistry, University of Pittsburgh, Pittsburgh, Pennsylvania 15260, United States;* orcid.org/0000-0003-0071-7127

Samantha T. Hung − *Department of Chemistry, Stanford University, Stanford, California 94305, United States;* orcid.org/0000-0001-9448-0962

Nhu Dao − *Department of Chemistry, Stanford University, Stanford, California 94305, United States; Science Learning Institute, Foothill College, Los Altos Hills, California 94022, United States*

Jordyn N. S. Smith − *Department of Chemistry, Stanford University, Stanford, California 94305, United States;* orcid.org/0009-0005-1522-8862

Complete contact information is available at: https://pubs.acs.org/10.1021/acs.jpcb.4c08739

Author Contributions

‖J.P. and K.A.C.-F. contributed equally to this paper.

Notes

The authors declare no competing financial interest.

ACKNOWLEDGMENTS

This work was supported by the National Science Foundation, Division of Chemistry, Award Number 1954392. K.A.C.-F. was supported by a Stanford Science Fellowship.

REFERENCES

(1) Clarke, C. J.; Tu, W.-C.; Levers, O.; Bröhl, A.; Hallett, J. P. Green and Sustainable Solvents in Chemical Processes. *Chem. Rev.* **2018**, *118*, 747−800.

(2) Kerton, F.; Marriott, R. *Alternative Solvents for Green Chemistry*; Royal Society of chemistry, 2013. .

(3) Lewis, A. C.; Hopkins, J. R.; Carslaw, D. C.; Hamilton, J. F.; Nelson, B. S.; Stewart, G.; Dernie, J.; Passant, N.; Murrells, T. An increasing role for solvent emissions and implications for future measurements of volatile organic compounds. *Philos. Trans. R. Soc., A* **2020**, *378*, 20190328.

(4) McDonald, B. C.; de Gouw, J. A.; Gilman, J. B.; Jathar, S. H.; Akherati, A.; Cappa, C. D.; Jimenez, J. L.; Lee-Taylor, J.; Hayes, P. L.; McKeen, S. A.; et al. Volatile chemical products emerging as largest petrochemical source of urban organic emissions. *Science* **2018**, *359*, 760−764.

(5) Jessop, P. G. Searching for green solvents. *Green Chem.* **2011**, *13*, 1391−1398.

(6) Reichardt, C.; Welton, T. *Solvents and Solvent Effects in Organic Chemistry*; Wiley-VCH, 2011.

(7) Dyson, P. J.; Jessop, P. G. Solvent effects in catalysis: Rational improvements of catalysts via manipulation of solvent interactions. *Catal. Sci. Technol.* **2016**, *6*, 3302−3316.

(8) Maldonado, A. M.; Basdogan, Y.; Berryman, J. T.; Rempe, S. B.; Keith, J. A. First-principles modeling of chemistry in mixed solvents: Where to go from here? *J. Chem. Phys.* **2020**, *152* (13), 130902.

(9) Hansen, B. B.; Spittle, S.; Chen, B.; Poe, D.; Zhang, Y.; Klein, J. M.; Horton, A.; Adhikari, L.; Zelovich, T.; Doherty, B. W.; et al. Deep Eutectic Solvents: A Review of Fundamentals and Applications. *Chem. Rev.* **2021**, *121*, 1232−1285.

(10) Srinivasan, H.; Sharma, V. K.; Mitra, S. Can. the microscopic and macroscopic transport phenomena in deep eutectic solvents be reconciled? *Phys. Chem. Chem. Phys.* **2021**, *23*, 22854−22873.

(11) Smith, E. L.; Abbott, A. P.; Ryder, K. S. Deep eutectic solvents (DESs) and their applications. *Chem. Rev.* **2014**, *114*, 11060−11082.
(12) Zhang, Q.; De Oliveira Vigier, K.; Royer, S.; Jerome, F. Deep eutectic solvents: Syntheses, properties and applications. *Chem. Soc. Rev.* **2012**, *41*, 7108−7146.
(13) Spittle, S.; Alfurayj, I.; Hansen, B. B.; Glynn, K.; Brackett, W.; Pandian, R.; Burda, C.; Sangoro, J. Enhanced Dynamics and Charge Transport at the Eutectic Point: A New Paradigm for the Use of Deep Eutectic Solvent Systems. *JACS Au* **2023**, *3*, 3024−3030.
(14) Cui, Y.; Fulfer, K. D.; Ma, J.; Weldeghiorghis, T. K.; Kuroda, D. G. Solvation dynamics of an ionic probe in choline chloride-based deep eutectic solvents. *Phys. Chem. Chem. Phys.* **2016**, *18*, 31471−31479.
(15) Pandey, A.; Pandey, S. Solvatochromic probe behavior within choline chloride-based deep eutectic solvents: Effect of temperature and water. *J. Phys. Chem. B* **2014**, *118*, 14652−14661.
(16) Hossain, S. S.; Samanta, A. How do the hydrocarbon chain length and hydroxyl group position influence the solute dynamics in alcohol-based deep eutectic solvents? *Phys. Chem. Chem. Phys.* **2018**, *20*, 24613−24622.
(17) Turner, A. H.; Kim, D. Rotation and translation dynamics of coumarin 153 in choline chloride-based deep eutectic solvents. *J. Chem. Phys.* **2018**, *149* (17), 174503.
(18) Chowdhury, T.; Chatterjee, S.; Deshmukh, S. H.; Bagchi, S. A Systematic Study on the Role of Hydrogen Bond Donors in Dictating the Dynamics of Choline-Based Deep Eutectic Solvents. *J. Phys. Chem. B* **2023**, *127*, 7299−7308.
(19) Malik, A.; Kashyap, H. K. Multiple evidences of dynamic heterogeneity in hydrophobic deep eutectic solvents. *J. Chem. Phys.* **2021**, *155* (4), 044502.
(20) Ferreira, E. S. C.; Voroshylova, I. V.; Figueiredo, N. M.; Cordeiro, M. Molecular dynamic study of alcohol-based deep eutectic solvents. *J. Chem. Phys.* **2021**, *155* (6), 064506.
(21) Chatterjee, S.; Ghosh, D.; Haldar, T.; Deb, P.; Sakpal, S. S.; Deshmukh, S. H.; Kashid, S. M.; Bagchi, S. Hydrocarbon Chain-Length Dependence of Solvation Dynamics in Alcohol-Based Deep Eutectic Solvents: A Two-Dimensional Infrared Spectroscopic Investigation. *J. Phys. Chem. B* **2019**, *123*, 9355−9363.
(22) Spittle, S.; Poe, D.; Doherty, B.; Kolodziej, C.; Heroux, L.; Haque, M. A.; Squire, H.; Cosby, T.; Zhang, Y.; Fraenza, C.; Bhattacharyya, S.; et al. Evolution of microscopic heterogeneity and dynamics in choline chloride-based deep eutectic solvents. *Nat. Commun.* **2022**, *13* (1), 219.
(23) Di Pietro, M. E.; Hammond, O.; van den Bruinhorst, A.; Mannu, A.; Padua, A.; Mele, A.; Costa Gomes, M. Connecting chloride solvation with hydration in deep eutectic systems. *Phys. Chem. Chem. Phys.* **2021**, *23*, 107−111.
(24) Abbott, A. P.; Capper, G.; Davies, D. L.; Rasheed, R. K.; Tambyrajah, V. Novel solvent properties of choline chloride/urea mixtures. *Chem. Commun.* **2003**, 70−71.
(25) van den Bruinhorst, A.; Kollau, L. J. B. M.; Vis, M.; Hendrix, M. M. R. M.; Meuldijk, J.; Tuinier, R.; Esteves, A. C. C. From a eutectic mixture to a deep eutectic system via anion selection: Glutaric acid + tetraethylammonium halides. *J. Chem. Phys.* **2021**, *155* (1), 014502.
(26) Hou, X.; Feng, G.; Chen, Z.; Wu, H.; Zhao, H.; Cao, S.; Hallett, J. P. Tailoring a suitable partner system for cholinium cation to build effective solvents for biomass deconstruction. *Green Chem.* **2024**, *26*, 5977−5987.
(27) Khajavian, M.; Vatanpour, V.; Castro-Munoz, R.; Boczkaj, G. Chitin and derivative chitosan-based structures - Preparation strategies aided by deep eutectic solvents: A review. *Carbohydr. Polym.* **2022**, *275*, 118702.
(28) Smink, D.; Juan, A.; Schuur, B.; Kersten, S. R. A. Understanding the Role of Choline Chloride in Deep Eutectic Solvents Used for Biomass Delignification. *Ind. Eng. Chem. Res.* **2019**, *58*, 16348−16357.
(29) Häkkinen, R.; Abbott, A. Solvation of carbohydrates in five choline chloride-based deep eutectic solvents and the implication for cellulose solubility. *Green Chem.* **2019**, *21*, 4673−4682.
(30) Zhang, Y.; Poe, D.; Heroux, L.; Squire, H.; Doherty, B. W.; Long, Z.; Dadmun, M.; Gurkan, B.; Tuckerman, M. E.; Maginn, E. J. Liquid Structure and Transport Properties of the Deep Eutectic Solvent Ethaline. *J. Phys. Chem. B* **2020**, *124*, 5251−5264.
(31) Agieienko, V.; Buchner, R. Is ethaline a deep eutectic solvent? *Phys. Chem. Chem. Phys.* **2022**, *24*, 5265−5268.
(32) Abranches, D. O.; Coutinho, J. A. P. Everything You Wanted to Know about Deep Eutectic Solvents but Were Afraid to Be Told. *Annu. Rev. Chem. Biomol. Eng.* **2023**, *14*, 141−163.
(33) Rempe, S. B.; Pratt, L. R.; Hummer, G.; Kress, J. D.; Martin, R. L.; Redondo, A. The Hydration Number of Li+in Liquid Water. *J. Am. Chem. Soc.* **2000**, *122*, 966−967.
(34) Mancinelli, R.; Botti, A.; Bruni, F.; Ricci, M. A.; Soper, A. K. Hydration of sodium, potassium, and chloride ions in solution and the concept of structure maker/breaker. *J. Phys. Chem. B* **2007**, *111*, 13570−13577.
(35) Singh, M. B.; Dalvi, V. H.; Gaikar, V. G. Investigations of clustering of ions and diffusivity in concentrated aqueous solutions of lithium chloride by molecular dynamic simulations. *RSC Adv.* **2015**, *5*, 15328−15337.
(36) Kim, H.; Hong, J.; Park, K. Y.; Kim, H.; Kim, S. W.; Kang, K. Aqueous rechargeable Li and Na ion batteries. *Chem. Rev.* **2014**, *114*, 11788−11827.
(37) Shen, Y.; Liu, B.; Liu, X.; Liu, J.; Ding, J.; Zhong, C.; Hu, W. Water-in-salt electrolyte for safe and high-energy aqueous battery. *Energy Storage Mater.* **2021**, *34*, 461−474.
(38) Takamuku, T.; Yamamoto, M.; To, T.; Matsugami, M. Solvation Structures of Tetraethylammonium Bromide and Tetrafluoroborate in Aqueous Binary Solvents with Ethanol, Trifluoroethanol, and Acetonitrile. *J. Phys. Chem. B* **2020**, *124*, 5009−5020.
(39) Gurkan, B.; Squire, H.; Pentzer, E. Metal-Free Deep Eutectic Solvents: Preparation, Physical Properties, and Significance. *J. Phys. Chem. Lett.* **2019**, *10*, 7956−7964.
(40) Tamimi, A.; Fayer, M. D. Ionic Liquid Dynamics Measured with 2D IR and IR Pump-Probe Experiments on a Linear Anion and the Influence of Potassium Cations. *J. Phys. Chem. B* **2016**, *120*, 5842−5854.
(41) Karthick Kumar, S. K.; Tamimi, A.; Fayer, M. D. Comparisons of 2D IR measured spectral diffusion in rotating frames using pulse shaping and in the stationary frame using the standard method. *J. Chem. Phys.* **2012**, *137* (18), 184201.
(42) Frisch, M.; Trucks, G.; Schlegel, H. B.; Scuseria, G.; Robb, M.; Cheeseman, J.; Scalmani, G.; Barone, V.; Petersson, G.; Nakatsuji, H. *Gaussian 16*; Gaussian, Inc: Wallingford, CT, 2016.
(43) Marenich, A. V.; Cramer, C. J.; Truhlar, D. G. Universal solvation model based on solute electron density and on a continuum model of the solvent defined by the bulk dielectric constant and atomic surface tensions. *J. Phys. Chem. B* **2009**, *113*, 6378−6396.
(44) Yamada, S. A.; Thompson, W. H.; Fayer, M. D. Water-anion hydrogen bonding dynamics: Ultrafast IR experiments and simulations. *J. Chem. Phys.* **2017**, *146* (23), 234501.
(45) Yuan, R.; Yan, C.; Tamimi, A.; Fayer, M. D. Molecular Anion Hydrogen Bonding Dynamics in Aqueous Solution. *J. Phys. Chem. B* **2015**, *119*, 13407−13415.
(46) Tan, H.-S.; Piletic, I. R.; Fayer, M. D. Polarization selective spectroscopy experiments: Methodology and pitfalls. *J. Opt. Soc. Am. B* **2005**, *22* (9), 2009−2017.
(47) Tokmakoff, A. Orientational correlation functions and polarization selectivity for nonlinear spectroscopy of isotropic media. I. Third order. *J. Chem. Phys.* **1996**, *105*, 1−12.
(48) Kenkre, V. M.; Tokmakoff, A.; Fayer, M. D. Theory of vibrational relaxation of polyatomic molecules in liquids. *J. Chem. Phys.* **1994**, *101*, 10618−10629.
(49) Lenchenkov, V.; She, C.; Lian, T. Vibrational relaxation of CN stretch of pseudo-halide anions (OCN-, SCN-, and SeCN-) in polar solvents. *J. Phys. Chem. B* **2006**, *110*, 19990−19997.
(50) Lee, M. W.; Meuwly, M. On the role of nonbonded interactions in vibrational energy relaxation of cyanide in water. *J. Phys. Chem. A* **2011**, *115*, 5053−5061.

https://doi.org/10.1021/acs.jpcb.4c08739
J. Phys. Chem. B XXXX, XXX, XXX−XXX

(51) Rey, R.; Hynes, J. T. Vibrational phase and energy relaxation of CN− in water. *J. Chem. Phys.* **1998**, *108*, 142−153.
(52) Xing, X.; Li, J.; Breen, J. P.; Nishida, J.; Karunadasa, H. I.; Fayer, M. D. Probing Lattice Dynamics in Two-Dimensional Inorganic Pseudohalide Perovskites with Ultrafast Infrared Spectroscopy. *J. Phys. Chem. C* **2022**, *126*, 10145−10158.
(53) Chatterjee, S.; Deshmukh, S. H.; Bagchi, S. Does Viscosity Drive the Dynamics in an Alcohol-Based Deep Eutectic Solvent? *J. Phys. Chem. B* **2022**, *126*, 8331−8337.
(54) Moilanen, D. E.; Fenn, E. E.; Lin, Y. S.; Skinner, J. L.; Bagchi, B.; Fayer, M. D. Water inertial reorientation: Hydrogen bond strength and the angular potential. *Proc. Natl. Acad. Sci. U. S. A.* **2008**, *105*, 5295−5300.
(55) Moog, R. S.; Ediger, M. D.; Boxer, S. G.; Fayer, M. D. Viscosity dependence of the rotational reorientation of rhodamine B in mono- and polyalcohols. Picosecond transient grating experiments. *J. Phys. Chem.* **1982**, *86*, 4694−4700.
(56) Becker, S. R.; Poole, P. H.; Starr, F. W. Fractional Stokes-Einstein and Debye-Stokes-Einstein relations in a network-forming liquid. *Phys. Rev. Lett.* **2006**, *97*, 055901.
(57) Tan, H. S.; Piletic, I. R.; Fayer, M. D. Orientational dynamics of water confined on a nanometer length scale in reverse micelles. *J. Chem. Phys.* **2005**, *122* (17), 174501.
(58) Lipari, G.; Szabo, A. Model-free approach to the interpretation of nuclear magnetic resonance relaxation in macromolecules. 1. Theory and range of validity. *J. Am. Chem. Soc.* **1982**, *104*, 4546−4559.
(59) Lipari, G.; Szabo, A. Effect of librational motion on fluorescence depolarization and nuclear magnetic resonance relaxation in macromolecules and membranes. *Biophys. J.* **1980**, *30*, 489−506.
(60) Wang, C. C.; Pecora, R. Time-correlation functions for restricted rotational diffusion. *J. Chem. Phys.* **1980**, *72*, 5333−5340.
(61) Kramer, P. L.; Giammanco, C. H.; Fayer, M. D. Dynamics of water, methanol, and ethanol in a room temperature ionic liquid. *J. Chem. Phys.* **2015**, *142* (21), 212408.
(62) Pan, J.; Charnay, A. P.; Fica-Contreras, S. M.; Fayer, M. D. Restricted Orientation Anisotropy Method for FVE Radii Characterization: Confirmed and Refined via the Study of Six Vibrational Probes. *Macromolecules* **2024**, *57*, 903−915.
(63) Roget, S. A.; Heck, T. R.; Carter-Fenk, K. A.; Fayer, M. D. Ion/Water Network Structural Dynamics in Highly Concentrated Lithium Chloride and Lithium Bromide Solutions Probed with Ultrafast Infrared Spectroscopy. *J. Phys. Chem. B* **2023**, *127*, 4532−4543.
(64) Hoffman, D. J.; Fica-Contreras, S. M.; Fayer, M. D. Amorphous polymer dynamics and free volume element size distributions from ultrafast IR spectroscopy. *Proc. Natl. Acad. Sci. U. S. A.* **2020**, *117*, 13949−13958.

https://doi.org/10.1021/acs.jpcb.4c08739
J. Phys. Chem. B XXXX, XXX, XXX−XXX